Journal of Alloys and Compounds 877 (2021) 160268

Contents lists available at ScienceDirect

Journal of Alloys and Compounds

journal homepage: www.elsevier.com/locate/jalcom

# Improvement of ductility and work hardening ability in a high strength Zn-Mg-Y alloy via micron-sized and submicron-sized $YZn_{12}$ particles

He Huang[a], Huan Liu[a,*], Kangxuan Ren[a], Jiahui Shi[b], Jia Ju[c], Haoran Wu[a], Jinghua Jiang[a], Aibin Ma[a], Feng Xue[d], Jing Bai[d,*], Yufeng Zheng[b,*]

[a] College of Mechanics and Materials, Hohai University, Nanjing 210000, China
[b] Academy for Advanced Interdisciplinary Studies, Peking University, Beijing 100871, China
[c] College of Materials Engineering, Nanjing Institute of Technology, Nanjing 211167, China
[d] College of Materials Science and Engineering, Southeast University, Nanjing 211189, China

ARTICLE INFO

*Article history:*
Received 21 March 2021
Received in revised form 28 April 2021
Accepted 29 April 2021
Available online 8 May 2021

*Keywords:*
Zn-Mg-Y alloy
Equal channel angular pressing
Ductility
Work hardening

ABSTRACT

In this study, the effects of Y addition on microstructure and mechanical properties of Zn-Mg alloy during multi-pass equal channel angular pressing (ECAP) were systematically investigated. The results show that apart from α-Zn matrix and network-shaped eutectic Zn+$Mg_2Zn_{11}$ structure, micron-sized and submicron-sized $YZn_{12}$ particles were formed in as-cast alloy. During multi-pass ECAP, the α-Zn matrix was refined via dynamic recrystallization (DRX), and the eutectic structure was fragmented into fine particles gradually, while the $YZn_{12}$ particles became further refined (~100 nm) only from 8p to 12p ECAP. Tensile tests at room temperature indicated that the 12p-ECAP alloy exhibits the optimal mechanical properties with ultimate tensile strength of 465 MPa and fracture elongation of 11%. The fine and uniform microstructure contributes to the enhancement of ductility. Furthermore, the improved work hardening ability of 12p alloy was mainly ascribed from the generation of submicron-sized $YZn_{12}$ particles with the size of ~100 nm, which could induce twinning with them and increase the density of geometrically necessary dislocations. The results suggest that the introduction of second phase particles with twinning ability may be effective to improve the work hardening ability of Zn alloys.

© 2021 Elsevier B.V. All rights reserved.

## 1. Introduction

Zn and its alloys have been accepted as promising biodegradable metallic materials (BMMs) owing to their appropriate degradable rate (between Mg and Fe) and good biocompatibility [1,2]. However, the mechanical properties of pure Zn are so inferior that it fails to meet the mechanical requirements of BMMs [3]. Therefore, much work has been done in recent years to improve the mechanical properties of Zn alloys. It is found that Zn-Mg alloys containing a high volume fraction of eutectic structure can achieve ultra-high strength through the thermomechanical process [4–6]. Nevertheless, when Zn-Mg alloys undergo cold working, microcracks will generate from the Zn/$Mg_2Zn_{11}$ interface due to the mismatch of deformation abilities between the soft Zn matrix and hard $Mg_2Zn_{11}$ phase, resulting in poor ductility and fracture toughness for the alloys. Moreover, the occurrence of strain-softening in most Zn alloys was attributed to recrystallization when they underwent tensile process at room temperature, which, unfortunately, would result in non-uniform deformation of biomedical counterparts in the course of their service [7]. Therefore, it is essential to improve the ductility and work hardening ability of ultra-high strength Zn alloys for the purpose of expanding their applications.

Addition of third elements in Zn-X (X=Li, Mg, Cu, Mn and so on) has a significant influence on the microstructure and mechanical properties of Zn alloys. For instance, Yang et al. [8] found that the elongation of Zn-0.8Li (wt%) alloys with a high volume fraction of second phase was increased by adding Mn element. This was attributed to the introduction of the $MnZn_{13}$ phase, which could alleviate stress concentration around them via forming twinning structure during the thermomechanical process [9]. Oppositely, Zn-Mg-Ca alloys reported by Huang et al. [10] possess poor ductility owing to the formation of brittle $CaZn_{13}$ particles, which were broken and became pre-cracks during multi-pass equal channel angular process (ECAP). In another research [11], the $CaZn_{13}$ phase can be refined and distributed uniformly via extrusion of annealed materials, resulting in larger elongation compared with extrusion of

* Corresponding authors.
*E-mail addresses:* liuhuanseu@hhu.edu.cn (H. Liu), baijing@seu.edu.cn (J. Bai), yfzheng@pku.edu.cn (Y. Zheng).

https://doi.org/10.1016/j.jallcom.2021.160268
0925-8388/© 2021 Elsevier B.V. All rights reserved.

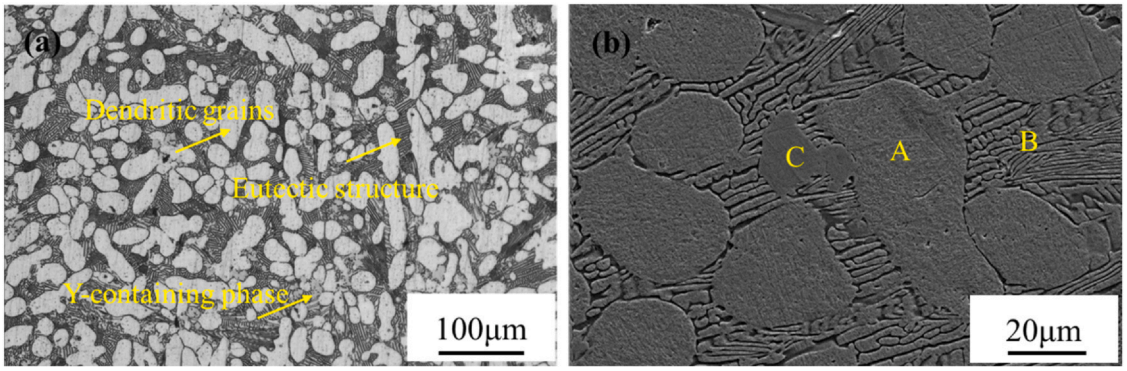


**Fig. 1.** Microstructure of as-cast Zn-Mg-Y alloy: (a) optical image, (b) SEM image.

as-cast materials. Meanwhile, the second phase with different sizes has an important influence on boundary slip, which is determined to recrystallization process [12]. Therefore, refining and obtaining deformed particles in Zn alloys with high strength will benefit their elongation and work hardening rates.

Rare-earth elements play a critical role in enhancing the mechanical properties of Mg alloys [13], and some Mg alloys containing rare-earth elements, i.e. WE43, possess good biocompatibility as well [14–16]. Shi et al. [17] first employed combined additions of Y and Nd elements in Zn-1Mn-0.1Fe alloys to serve as nucleating agents of (Fe, Mn)$Zn_{13}$ particles by forming RE-rich intermetallic compounds. They confirmed that the Zn-Mn-Fe-Y-Nd alloy not only showed good biocompatibility with cell viabilities higher than the threshold of 70%, but also stimulated cell proliferation with cell viabilities higher than 100%, demonstrating the good biocompatibility of Zn alloys with the addition of Y and Nd element. So far, no research on addition of Y in Zn-Mg based alloys has been reported. Therefore, concerning the biocompatibility of rare-earth element Y and its potential strengthening effect, minor Y was induced into Zn-1.5Mg (wt%) alloy in this study, and the ECAP was selected as the subsequent thermomechanical process. By characterizing the microstructure and measuring the mechanical properties of the Zn-Mg-Y alloys, the effects of the Y element on the microstructure evolution and mechanical properties of Zn-Mg alloys during the ECAP process were investigated.

## 2. Experiment procedure

The raw materials, including pure Zn (99.90 wt%), pure Mg (99.95 wt%) metals and Mg-30Y (wt%) master alloys, were employed to prepare as-cast Zn-1.5Mg-0.3Y (wt%) alloy ingot. After melting in a low-carbon steel crucible under the protection of a mixed atmosphere of $CO_2$ and $SF_6$ (99:1), the molten metal was poured into a steel mould with an inner the dimension of 200 mm × 70 mm × 25 mm, cooled naturally to room temperature. Before melting, the crucible and all iron tools were covered with a protective layer via the mixture consisting of zinc oxide, sodium silicate and deionized water (mass ratio of 3:1:6). Cuboid samples with dimension of 20 mm × 20 mm × 45 mm were then cut from the ingot for subsequent plastic processing. ECAP process was carried out at 150 °C in a rotary die (RD). The schematic diagram and detailed information of the RD-ECAP were described in our former studies [18,19]. The rotary die consists of a cross channel with four sliding blocks, and the major advantage of this rotary die is that multi-pass RD-ECAP could be easily realized by rotating the die to 90 ° between two successive ECAP passes without taking the sample out and in after each pass of pressing [20]. In the current study, the ECAP numbers were set as 4, 8 and 12, respectively. Before the first pass, the sample and rotary die were kept at 150 °C for 60 min. Then every four passes of ECAP, the die and the sample together were reheated and kept at 150 °C for 10 min

The microstructure of as-cast and ECAP alloys was characterized by an Olympus BHM optical metallographic microscope (OM) and a Sirion field-emission scanning electron microscope (SEM) equipped with a GENESIS 60 S X-ray energy spectrometer (EDS). The metallographic and SEM samples were prepared by mechanical grinding, polishing and etching (the etchant was 4 wt% nitric acid in alcoholic solution). To further investigate the morphology of second phases and DRX grains, TEM observations were conducted by a Tecnai G2 transmission electron microscope. The TEM samples were prepared by twin-jet electron-polishing in a 4 wt% perchloric acid alcohol solution. Moreover, the ECAP samples were also characterized by the electron backscattered diffraction (EBSD) analysis, and the measured data were analyzed by Channel 5 software to evaluate the grain size distribution, texture evolution and dislocation density.

Tensile tests of as-cast and ECAP alloys were carried out by a CMT-5105 electronic universal testing machine at room temperature at a strain rate of $1 \times 10^{-3}$ $s^{-1}$. Dog-bone tensile samples with the gauge dimension of 6 mm × 2.5 mm × 2 mm were cut from both as-cast and ECAP alloys with the loading direction parallel to the ECAP ram direction. Five parallel specimens were employed, and the mean values were calculated as tensile properties for each processing state.

## 3. Results

### 3.1. Microstructure of as-cast Zn-Mg-Y alloy

Fig. 1(a) shows the optical image of as-cast Zn-Mg-Y alloy. Dendritic grains (bright contrast), lamellar eutectic structure (dark contrast), as well as another grey phase, are observed in the as-cast alloy. The area fraction of the eutectic structure is estimated to be ~ 50% using Image-J software based on contrast differences. High-magnification SEM image (Fig. 1(b)) and the corresponding EDS results (listed in Table 1) show that the Y and Mg elements are mainly concentrated on the C region and B region (marked in Fig. 1(b)), respectively. According to Zn-Y and Zn-Mg binary phase diagram [21,22], the $YZn_{12}$ phase and $Mg_2Zn_{11}$ phase form near the Zn-rich corners. Compared with the EDS results, it can be confirmed that the

**Table 1**
EDS elemental content analysis of the as-cast Zn alloys.

| Area | Analyzed chemical composition (wt%) | | |
|---|---|---|---|
| | Zn | Mg | Y |
| A | 99.88 | 0.12 | 0.00 |
| B | 97.80 | 2.11 | 0.10 |
| C | 89.70 | 0.00 | 10.30 |

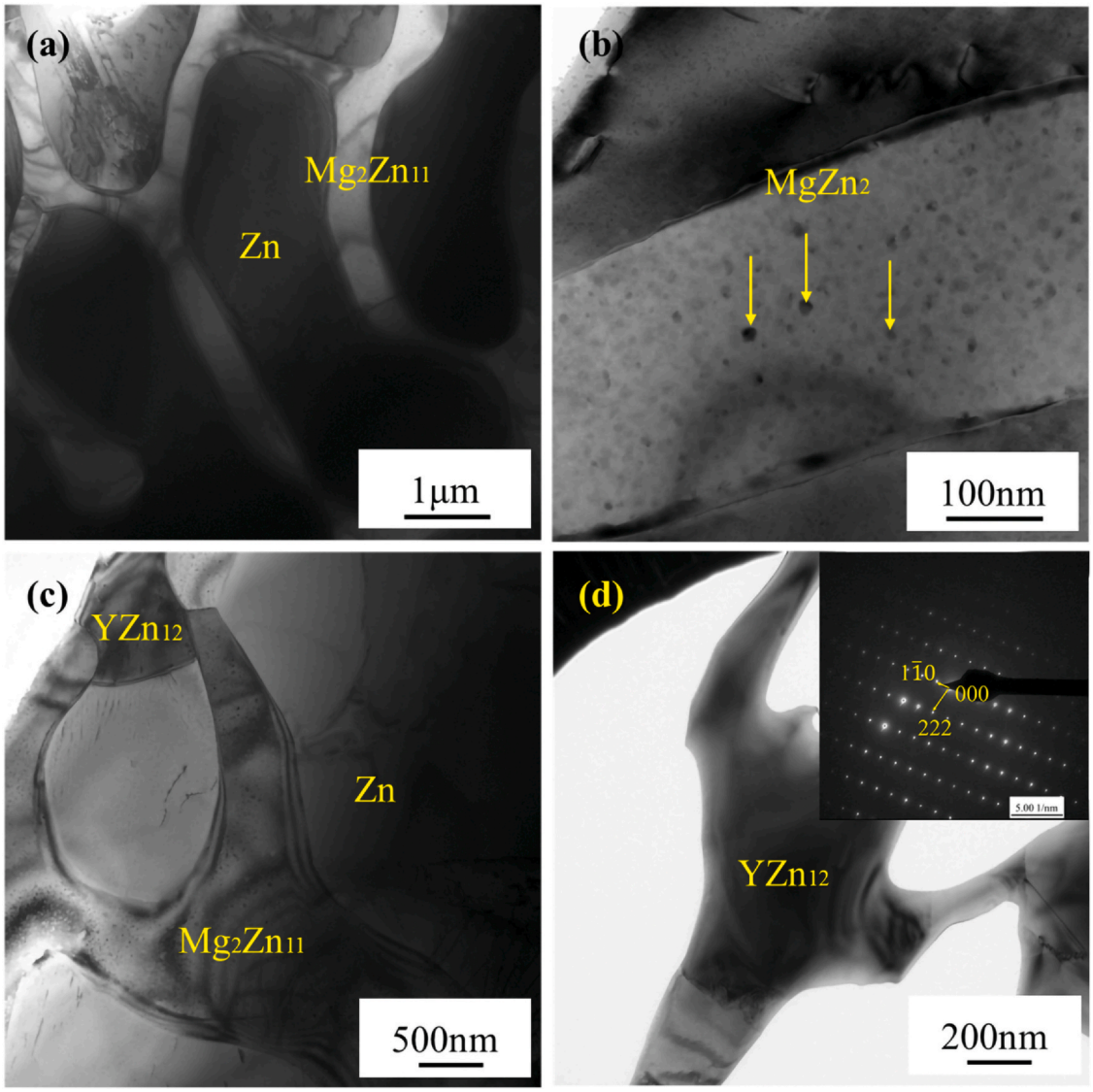


**Fig. 2.** TEM images of as-cast Zn-Mg-Y alloy: (a) eutectic structure; (b) nano-sized $MgZn_2$ particles within $Mg_2Zn_{11}$ grains; (c) submicron-sized$YZn_{12}$ phase; (d) micron-sized $YZn_{12}$ phase.

C region and B region represent $YZn_{12}$ phase and the Zn + $Mg_2Zn_{11}$ eutectic structure, respectively.

Fig. 2 shows the TEM observations of as-cast alloy. It can be found from Fig. 2(a) that the $Mg_2Zn_{11}$ phase exhibits network shape and alternative distribution with Zn grains. Moreover, a large number of nanosized $MgZn_2$ particles can be observed within the $Mg_2Zn_{11}$ phase (Fig. 2(b)). The detailed component information of the eutectic structure within Zn-Mg and Zn-Mg based alloys has been reported in our previous studies [10,23,24]. With regards to $YZn_{12}$ particles, Fig. 2(c) and (d) show that they exhibit two different sizes. One kind of $YZn_{12}$ particles is usually lower than 1 μm (Fig. 2(c); named as submicron-sized $YZn_{12}$ particles hereafter), and the other kind possesses larger size (Fig. 2(d); denoted as micron-sized $YZn_{12}$ particles). In addition, the submicron-sized $YZn_{12}$ particles are always located within the Zn+$Mg_2Zn_{11}$ eutectic structure, while the micron-sized $YZn_{12}$ particles could be found either within the eutectic or within Zn matrix.

### 3.2. Microstructure of ECAP Zn-Mg-Y alloys

Fig. 3 shows the SEM images and elements distribution maps of Zn-Mg-Y ECAP alloys. After 4 passes of processing, large grain regions are still observed, and a portion of the eutectic phase remains lamellar structure. With the increase ECAP passes, large grain regions gradually disappeared, and eutectic structure is fragmented into fine particles. Compared with 8p-ECAP and 12p-ECAP alloys, the distribution of the fragmented eutectic structure is more uniform after twelve passes of ECAP. Furthermore, as demonstrated by the distribution of Y element, it can be inferred that the micron-sized $YZn_{12}$ phase becomes finer and more uniform as increasing ECAP passes.

Fig. 4 shows the high magnification SEM images and corresponding EDS results of the 4p-ECAP and 12p-ECAP Zn-Mg-Y alloys. It can be found from the EDS results that the mass weight of Y element within selected areas is closed to the Y concentration of $YZn_{12}$ phase in as-cast Zn-Mg-Y alloy. This demonstrates that the phase in selected area are $YZn_{12}$ phase. Moreover, there are many aggregative micron-sized $YZn_{12}$ phases observed in 4p-ECAP alloy, the interspace of the $YZn_{12}$ phase is smaller than that in the12p-ECAP alloy. These results indicate that the distribution of the micron-sized $YZn_{12}$ phase becomes more uniform after twelve passes of ECAP.

Fig. 5 shows that the evolution of the submicron-sized $YZn_{12}$ phase in Zn-Mg-Y alloys processed by ECAP with different passes. After 8 passes of ECAP, a large number of $YZn_{12}$ particles close to

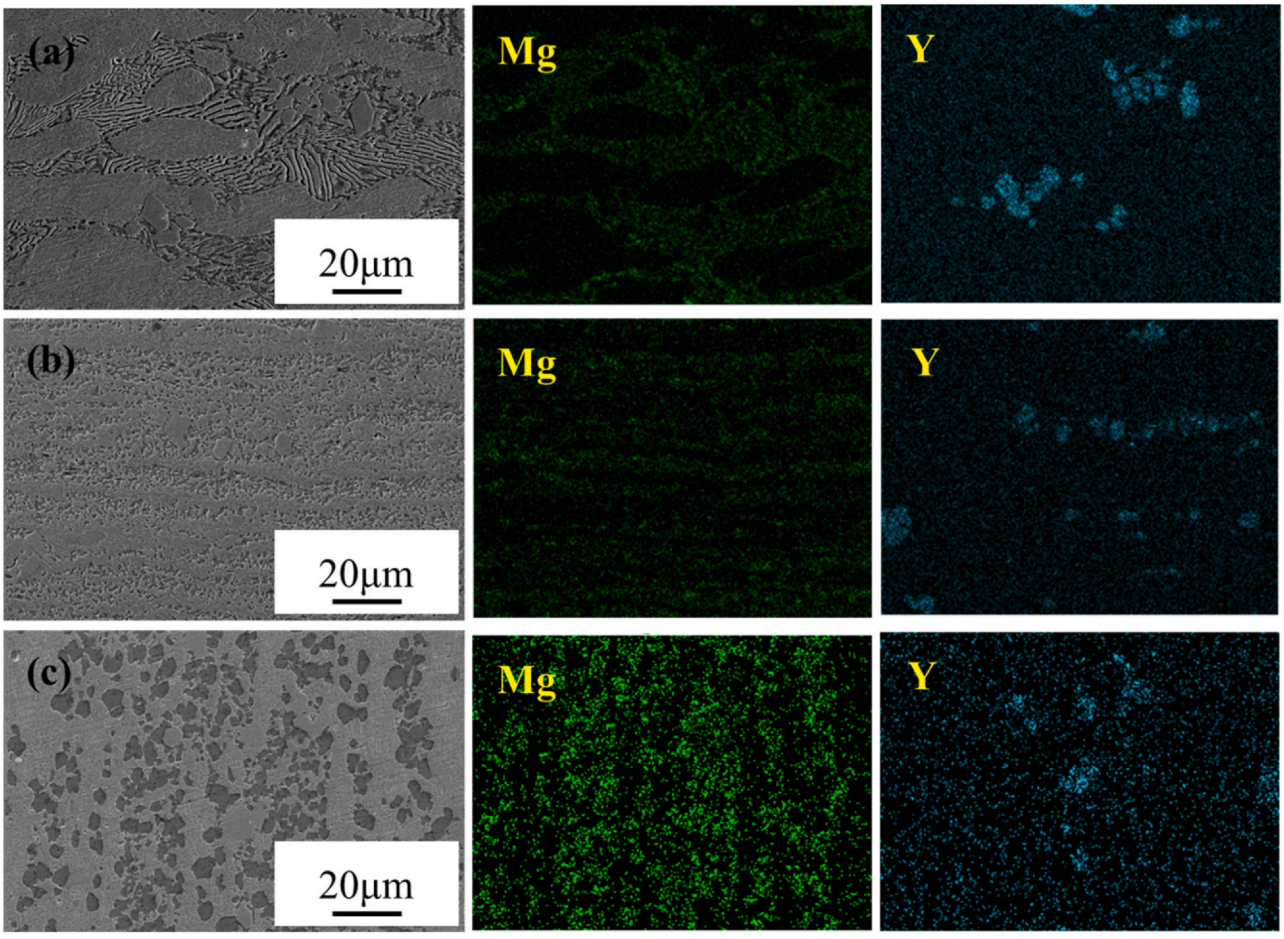


**Fig. 3.** Microstructure and elements distribution of Zn-Mg-Y alloy after ECAP: (a) 4p-ECAP, (b)8p-ECAP, (c) 12p-ECAP.

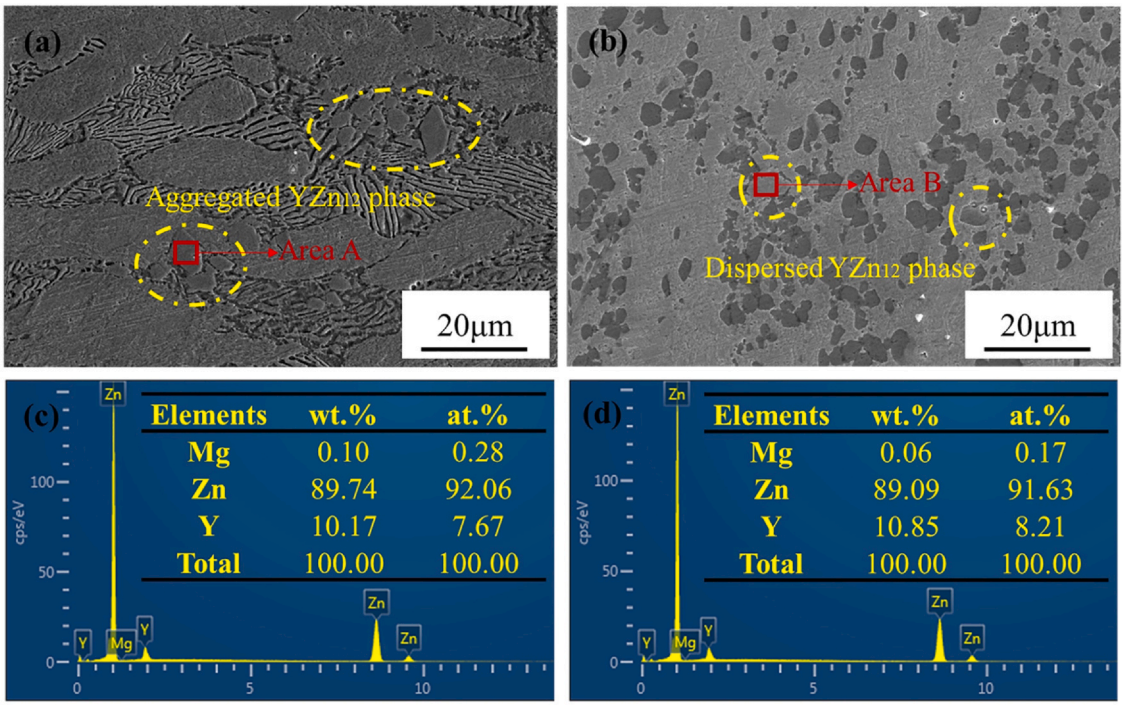


**Fig. 4.** The distribution of $YZn_{12}$ phase after ECAP process: (a) 4p-ECAP, (b) 12p-ECAP, EDS results in (c) area A and (d) area B.

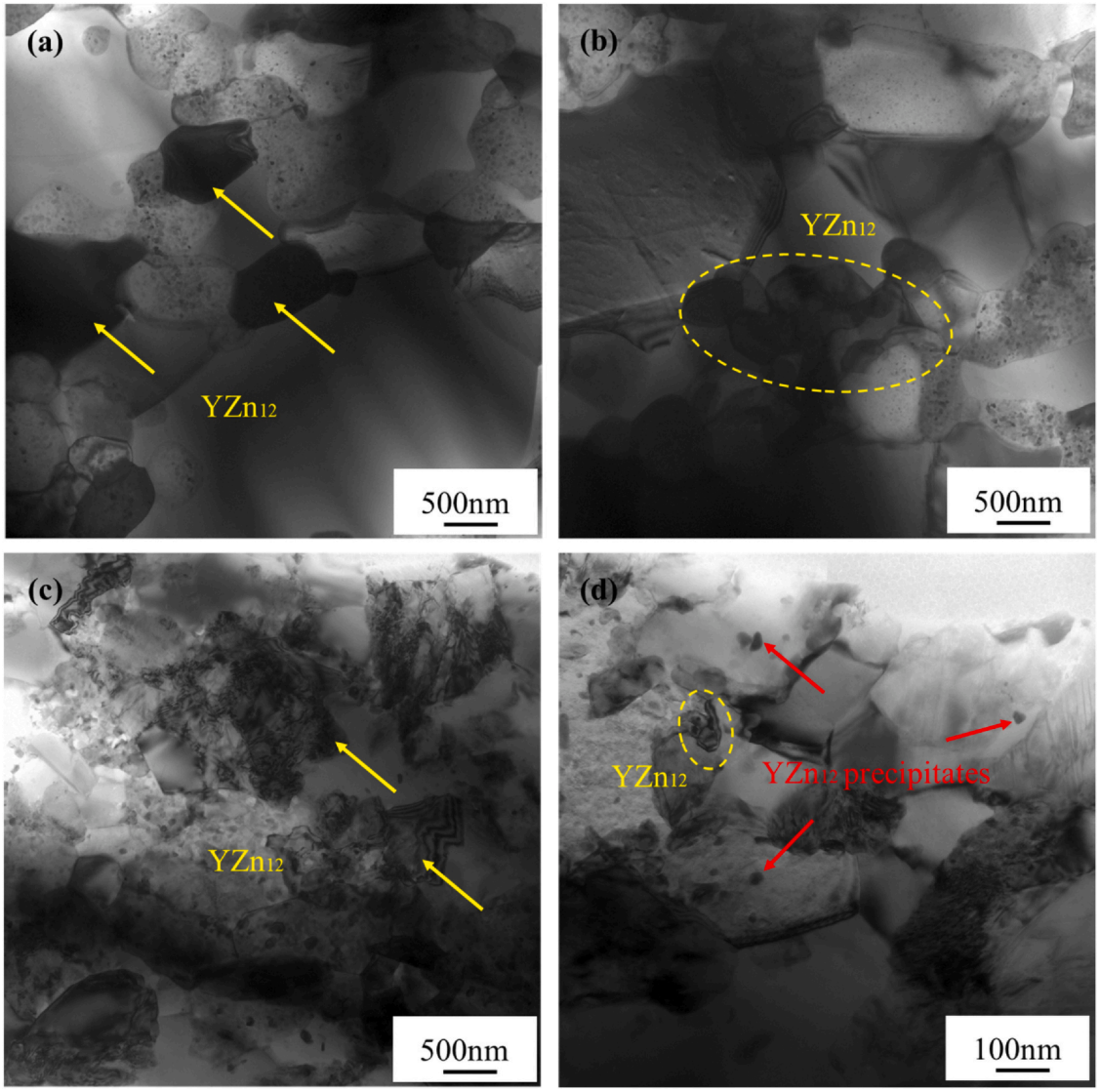


**Fig. 5.** TEM images of nanoscale $YZn_{12}$ phase in Zn-Mg-Y alloys processed by (a, b) 8p and (c, d)12p ECAP.

1 μm in size can be observed (as shown in Fig. 5(a)). The size of the submicron-sized $YZn_{12}$ particles in the 8p-ECAP alloy is similar to that in the as-cast alloy. Moreover, Fig. 5(b) shows the aggregation of submicron-sized $YZn_{12}$ phase. These findings indicate that eight passes of ECAP cannot effectively refine the submicron-sized $YZn_{12}$ phase distributed within the eutectic structure. Further increasing ECAP numbers, many $YZn_{12}$ phases smaller than 200 nm in size can be found, as shown in Fig. 5(c). It demonstrates that the size of the submicron-sized $YZn_{12}$ particles is refined after twelve passes of ECAP. In addition, some $YZn_{12}$ particles with diameter lower than 100 nm could be observed in Fig. 5(d). These nano-sized $YZn_{12}$ particles may be refined or even dynamically precipitated during 12 passes of ECAP, as the longer holding time at processing temperature could promote the dissolution of Y element and subsesquent large strains stimulate the precipitation of these particles.

### 3.3. Mechanical properties of Zn-Mg-Y alloys

The typical engineering stress-strain curves and detailed mechanical property values of as-cast and ECAP Zn-Mg-Y alloys are shown in Fig. 6(a) and (b), respectively. It can be observed that the tensile yield strength (YS) and the ultimate tensile strength (UTS) were improved obviously after ECAP, and 12p-ECAP alloy shows the highest strength together with good ductility (465 MPa and 11%, respectively). Increasing ECAP number from 4 to 8, although the strength was increased, the ductility is barely changed. However, a simultaneous improve of UTS and ductility occurred after 12 passes of ECAP (the TYS changed little compared with that of 8p-ECAP alloy), and there is distinct serration (as indicated by red circle) presented in its corresponding engineering stress vs. strain curve, suggesting twinning might happen. Moreover, the work-hardening rates of Zn-Mg-Y alloys were depicted in Fig. 6(c) and the value of $d\sigma/d\varepsilon$ is above zero until true strain reaches 11% for 12p-ECAP alloy, indicating that the 12p-ECAP Zn-Mg-Y alloy exhibits work-hardening behavior.

Table 2 shows the comparison between 12p-ECAP Zn-Mg-Y alloy and other reported Zn-Mg alloys [23–28]. Generally, the tensile strength of Zn-Mg alloys become higher with increasing Mg content. However, the high strength of Zn-Mg alloys is achieved at the expense of elongation. In the present study, 12p-ECAP Zn-Mg-Y alloy shows very high strength, which is very close to the highest strength of Zn-1.6Mg alloy processed by ECAP at 150 ℃, but the elongation is higher. Obviously, the mechanical properties are related to the microstructure evolution of Zn alloys. After ECAP, the microstructure of Zn-Mg-Y alloy has been refined and the refined microstructure is more uniform with increasing ECAP passes compared with Zn-1.6Mg

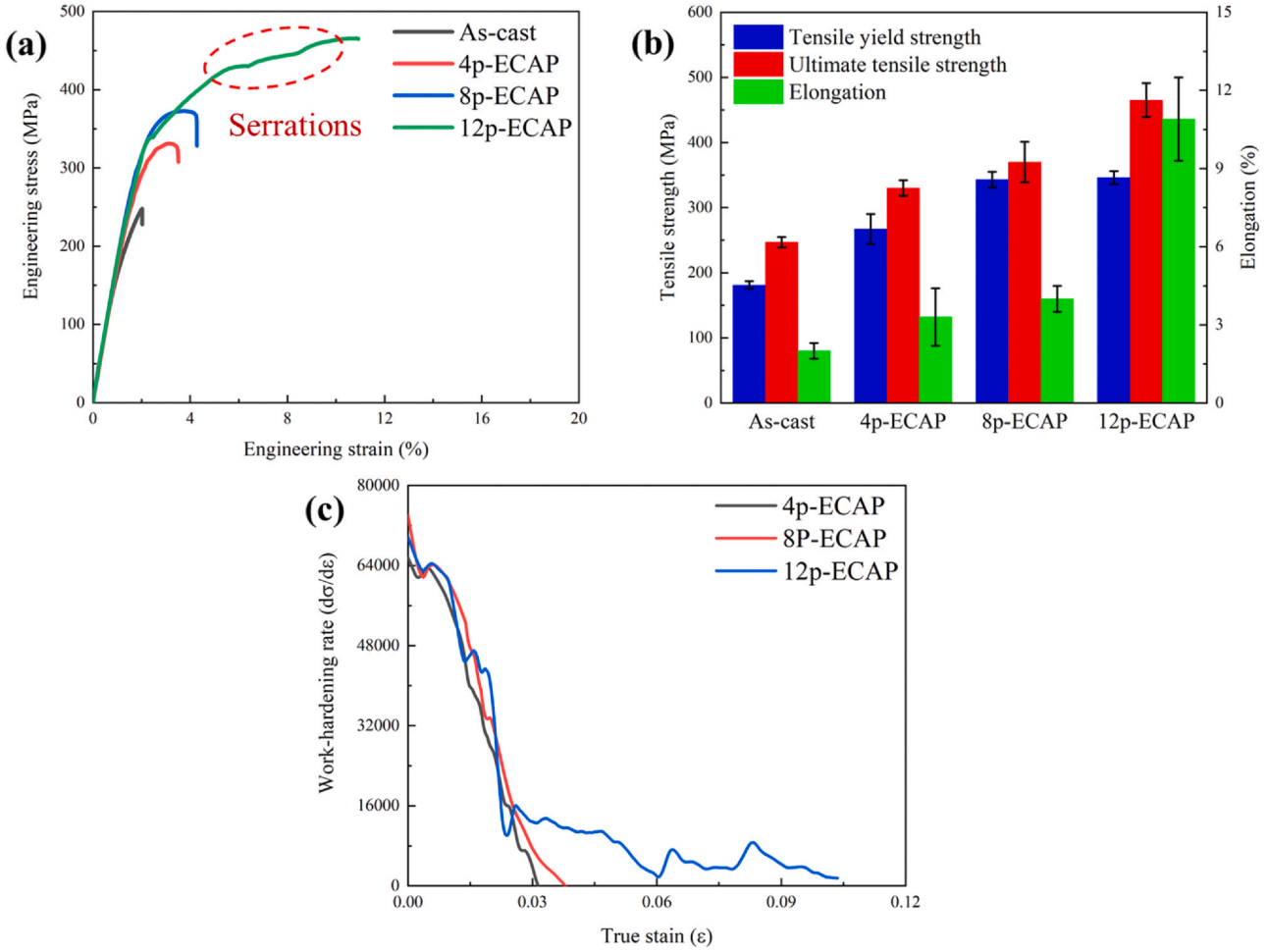


**Fig. 6.** Tensile mechanical properties of as-cast and ECAP Zn-Mg-Y alloys: (a) Engineering stress-strain curves, (b) column image of mechanical properties, (c) work-hardening rates curves.

**Table 2**
Comparison of mechanical properties of Zn-Mg alloys.

| Alloys (wt%) | Process states | UTS (MPa) | Elongation (%) | Reference |
|---|---|---|---|---|
| Zn-1.6Mg | HE[a] | 365 | 6 | [25] |
| Zn-1.6Mg | RS[b]+HE | 370 | 9 | [26] |
| Zn-3Mg | Tube extrusion | 399 | 1 | [27] |
| Zn-1.6Mg | ECAP (150 ℃) | 470 | 7 | [24] |
| Zn-1.6Mg | ECAP (200 ℃) | 407 | 4.8 | [23] |
| Zn-1.6Mg | ECAP (250 ℃) | 404 | 4.5 | [23] |
| Zn-0.4Mg | Rolling | 230 | 23 | [28] |
| Zn-0.8Mg | Rolling | 269 | 7.2 | [28] |
| Zn-1.5Mg-0.3Y | ECAP (150 ℃) | 465 | 10.9 | This study |

[a] HE is hot extrusion.
[b] RS is rapid solidification.

alloy. Therefore, it can be referred that the Y element plays an essential role in improving the ductility of high-strength Zn-Mg-Y alloys.

## 4. Discussions

### *4.1. The formation mechanism of $YZn_{12}$ phase with various sizes during solidification*

It is known from Fig. 2 that there are two types of $YZn_{12}$ phase, micron-sized $YZn_{12}$ particles and submicron-sized $YZn_{12}$ particles. The difference in size between the two $YZn_{12}$ particles is ralated to the nucleation and growth of the $YZn_{12}$ phase during solidification. According to Zn-Mg and Zn-Y binary phase diagram [21,22], the eutectic reactions, $L \rightarrow Zn + YZn_{12}$ and $L \rightarrow Zn + Mg_2Zn_{11}$, occurred at 685 ℃ and 364 ℃, respectively. Moreover, the appearance of nanoscale $MgZn_2$ phase indicates that the reaction $L \rightarrow MgZn_2$, may be occurred at around 580 ℃ owing to the local high concentration of Mg element. During cooling, these reactions occurred in sequence and resulted in the formation of different second phases. The generation of nanoscale $MgZn_2$ phase could be regarded as nucleation site to promote the nucleation in turn and contributes to the refinement of $YZn_{12}$ phase that formed within eutectic structure.

As for the subsequent growth of $YZn_{12}$ phase, it can be affected by surrounded lamellar eutectic structure. Due to the size difference between length and width of the lamellar-shaped eutectic structure, the growth of $YZn_{12}$ particles is affected by the boundary migration velocity. Hu et al. [29] reported that the grain growth rate could be calculated by the following Eq. (1):

$$v = M\gamma k(N-1)\exp\left(-C\frac{\varepsilon^*}{T(N-1)k}\right) \quad (1)$$

Where $M$ is a temperature-related coefficient, $N = \frac{K_a}{K}$ is grain-size-related dimensionless variable and K is mean curvature of individual grain, $\gamma$ is boundary energy, $k$ is Boltzmann's constant, $\varepsilon^*$ is defined as GB step free energy and $T$ is temperature. When the GB step free energy decrease to zero, the equation can be simplified as the Eq. (2):

$$v = M\gamma k(N-1) \quad (2)$$

Based on the Minkowski's theorem [30,31], the mean curvature of individual grain is inversely related with its mean caliper diameter, so the expression of $N$ can be expressed as $N = \frac{D}{D_a}$, where $D$ is mean diameter, $D_a$ is the mean diameter of adjacent grains. It can be referred that the value of $v$ increases with increasing $N$ value. In other words, the $YZn_{12}$ particles grow faster when they are adjacent to the long cross-section compared with short cross-section, which finally resulted in the appearance of micron-sized $YZn_{12}$ phase and submicron-sized$YZn_{12}$ phase.

### *4.2. The effect of $YZn_{12}$ phase on microstructure evolution of Zn-Mg-Y alloys during ECAP*

Similar to other second phases, the $YZn_{12}$ particles play a crucial role in the dynamic recrystallization (DRX) process of Zn alloys during hot processing. However, the effect of the $YZn_{12}$ particles with different sizes on DRX process is quite different. The formation of deformation zone around the micron-sized $YZn_{12}$ phase resulted in stress concentration and promoted the DRX process via particle stimulation nucleation (PSN) mechanism [32]. The submicron-sized $YZn_{12}$ phase, however, can inhibit the grain boundary movement, which negatively affects the DRX process. Fig. 7(a) and (b) show the EBSD recrystallization fraction maps of ECAP Zn-Mg-Y alloys. According to the average misorientation θ', the grains were classified into recrystallized (θ' ≤ 2°), substructured (2° < θ' < 7.5°), and deformed (θ' ≥ 7.5°) grains, and were marked by blue, yellow and red colors in Fig. 7, respectively [33]. It can be seen from Fig. 7(a) that there are some substructured grains with size larger than 20 μm, suggesting the recrystallization in 8p-ECAP alloy is not complete. As increasing ECAP passes, large grains disappeared (as shown in Fig. 7(b)). As indicated in Fig. 7(c), the recrystallization fraction in 8p-ECAP is close to that in 12p-ECAP. This is attributed to the refinement of micron-sized $YZn_{12}$ phase and the increased volume fraction of the submicron-sized $YZn_{12}$ phase after 12 passes of ECAP, among which the latter exhibited a negative effect on the DRX process. Moreover, the measured average grain sizes of 8p and 12p Zn-Mg-Y alloys shown in Fig. 7(d) are similar, 3.2 μm and 3.1 μm, respectively. According to the Hall-Petch relationship [34], the yield strength of metallic materials is inversely proportional to the square root of the average grain size. Consequently, it could be concluded that the similar yield strength of 8p-ECAP and 12p-ECAP alloy is attributed to the comparable average grain size.

It has been discussed in Fig. 3 that the eutectic structure and micron-sized $YZn_{12}$ phase are clearly refined after the ECAP process. In order to illustrate the refinement extent of eutectic structure and micron-sized $YZn_{12}$ phase, the high-magnification SEM images are shown in Fig. 8. The sizes of the fragmented eutectic structure and micron-sized $YZn_{12}$ phase were measured by Image-J software, and the statistic data were depicted in Fig. 8(d). The contrast between the Zn matrix and the second phases is close, so identifying the Zn matrix and second phases was achieved by EDS analysis. The micron-sized $YZn_{12}$ phase (as shown by the yellow arrows) and fragmented eutectic structure (as shown by the red arrows) contains high mass weight of the Y element and the Mg element, respectively. It can be calculated that the size of fragmented eutectic structure

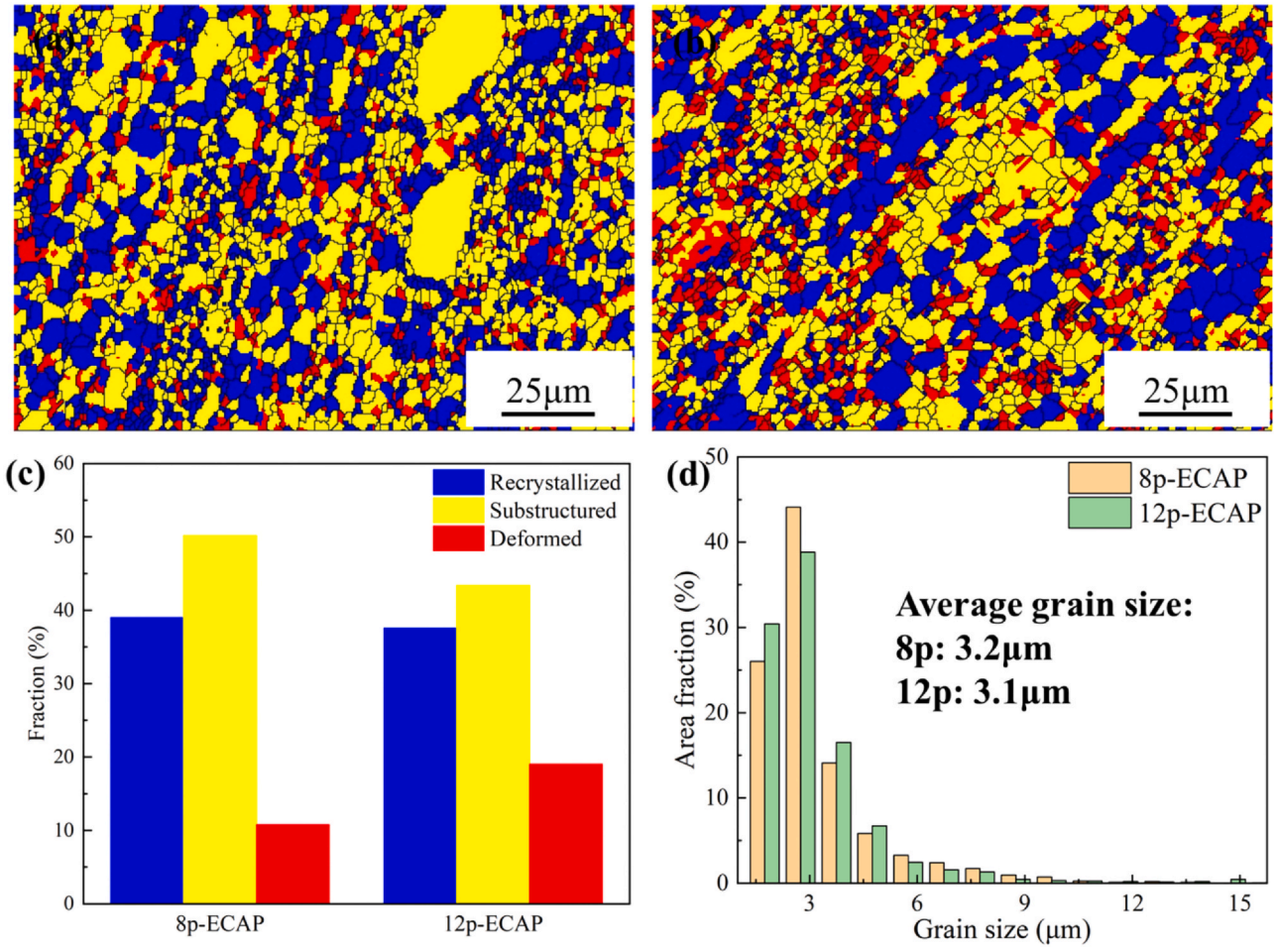


**Fig. 7.** EBSD recrystallization fraction maps of the Zn-Mg-Y alloys after ECAP: (a) 8p, (b) 12p, (c) statistics of recrystallization fraction, (d) average grain size.

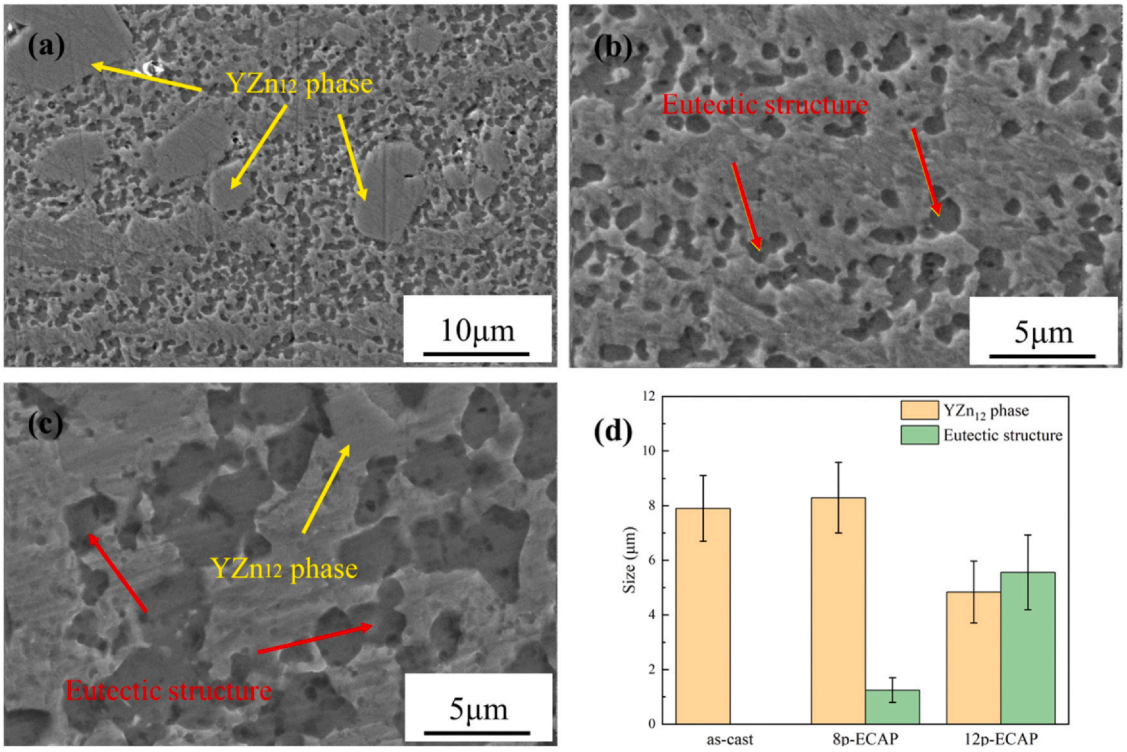


**Fig. 8.** The size evolution of second phases in ECAPed Zn-Mg-Y alloys: (a, b) 8p-ECAP, (c) 12p-ECAP, (d) second phases size statistics.

particles increased from 1.5 μm to 4 μm, while that of micron-sized $YZn_{12}$ phase decreased from 8 μm to 4 μm when passes of ECAP increased from 8 to 12.

As the fragmentation mechanism of eutectic structure in Zn-Mg and Zn-Mg based alloys is mechanical crushing [10,23], the extent of stress concentration will determine the size of the fragmented eutectic structure. The micron-sized $YZn_{12}$ phase in the 8p-ECAP alloy has a large size, it will cause a high level of stress concentration in the 8p-ECAP alloy. During the ECAP process, the stress concentration caused by the micron-sized $YZn_{12}$ phase will fragment the eutectic structure. However, keeping in the mould with longer time and releasing energy by the refinement of micron-sized $YZn_{12}$ phase will be regarded as the driving force to promote growth of $Mg_2Zn_{11}$ phase after twelve passes of ECAP. Therefore, it can be observed that the size of the fragmented eutectic structure in the 8p-ECAP alloy is even smaller than that in the 12p-ECAP alloy. Compared with sizes of Zn grains, fragmented eutectic structure and micron-sized $YZn_{12}$ phase, the size level among them is so equal in the 12p-ECAP alloy while differing from each other in the 8p-ECAP alloy. It will significantly affect the deformation compatibility of Zn alloys when they undergo tensile tests at room temperature. Moreover, the evolution of the nanoscale $MgZn_2$ phase (indicated by red arrows in Fig. 9) within the $Mg_2Zn_{11}$ phase shows no difference with other Zn-Mg alloys [23], suggesting that the appearance of the $YZn_{12}$ phase and growth of the $Mg_2Zn_{11}$ phase has little effect on the evolution of the nanoscale $MgZn_2$ phase.

### *4.3. Improvement of mechanical properties of Zn-Mg-Y alloys via ECAP process*

Dislocation slip and twinning are the main deformation modes for conventional metallic materials [35,36]. Texture plays a vital role in the ductility of metallic materials by affecting two deformation modes. Inverse pole figures (IPFs) and pole figures (PFs) of 8p and 12p alloys in Fig. 10 show that the texture direction in 8p alloy is parallel to the basal plane, while the texture direction in 12p alloy deviates from the basal plane. This deviation is attributed to the difference in texture in the large-grain (regarding grains with sizes more than 2 μm as large grain) domain because the recrystallisation textures of the two alloys are similar. Lou et al. [37] reported that the effect of texture evolution on mechanical properties in Zn-Mg-Mn alloys via extrusion at different temperatures. Their results showed that the ductility of Zn-Mg-Mn alloy extruded at 150 ℃ was higher than that extruded at 300 ℃, owing to the strong basal texture formed in Zn-Mg-Mn alloy extruded at higher temperature. Therefore, the ductility of the 8p-ECAP alloy is lower than that of the 12p-ECAP alloy can be attributed to the existence of the strong basal texture.

In addition, as shown in Fig. 11(a), twinning can be observed within the Zn matrix. Owing to the high c/a ratio of Zn, the twinning mode was contracted, and only the $\{10\bar{1}2\} < 10\bar{1}\bar{1}>$ twins can be activated [38–40]. The appearance of twins can alter the hard orientation of slip systems to promote dislocations slip during the ECAP process. Moreover, twins in the Zn matrix can improve the tensile strength of Zn alloys via inhibiting the movement of dislocations and lead to the occurrence of serration in the plastic flow stages like to that in twinning-induced plasticity (TWIP) steels [41,42]. In previous research on Zn-Mn alloys [43], ultimate tensile strength (UTS) of Zn-Mn alloys decreased from 220 MPa to 182 MPa as increasing Mn content, which was ascribed from the high-volume fraction of twins in Zn-0.2Mn alloy. Moreover, twins can also be observed in the refined submicron-sized $YZn_{12}$ phase, as shown in Fig. 11(b). Similar to the $MnZn_{13}$ phase [44], the appearance of twins in the refined submicron-sized $YZn_{12}$ phase can reduce stress concentration at the interface between the $YZn_{12}$ phase and Zn grains and $Mg_2Zn_{11}$ phase. However, it is worth noting that the size of the further refined submicron-sized $YZn_{12}$ particles with twins (around 100 nm) is usually smaller than that of submicron-sized $YZn_{12}$ phase. No twins can be observed in the original submicron-sized $YZn_{12}$ particles (~500 nm) and micron-sized $YZn_{12}$ particles. Based on the evolution of the $YZn_{12}$ phase in 8p-ECAP and 12p-ECAP alloys, it can be found that the refinement of submicron-sized $YZn_{12}$ phase is

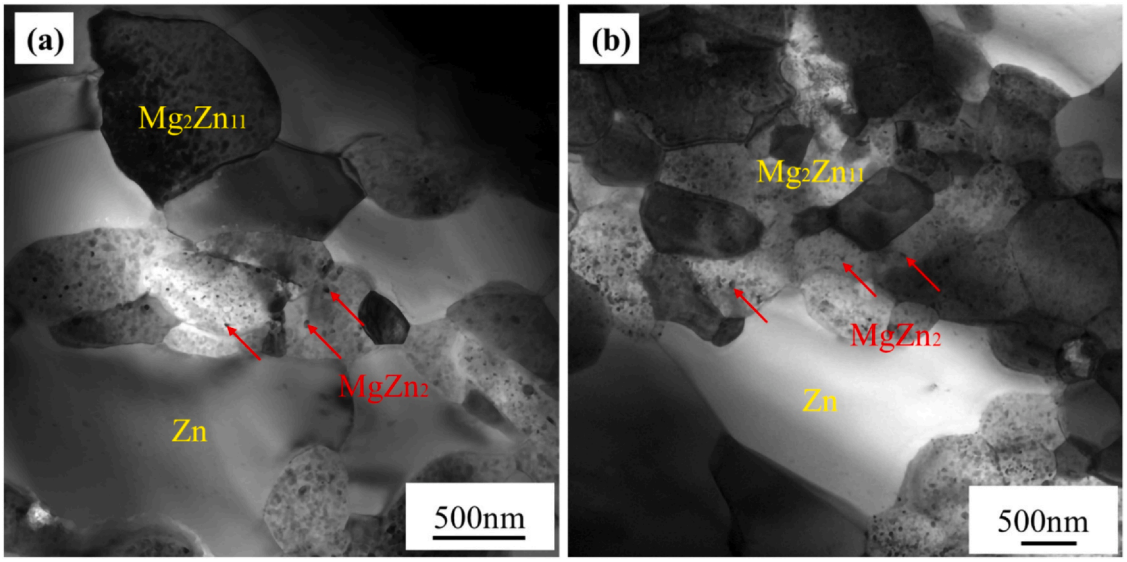


**Fig. 9.** TEM images of nanoscale $MgZn_2$ phase within $Mg_2Zn_{11}$ phase in (a) 8p-ECAP, (b) 12p-ECAP alloys.

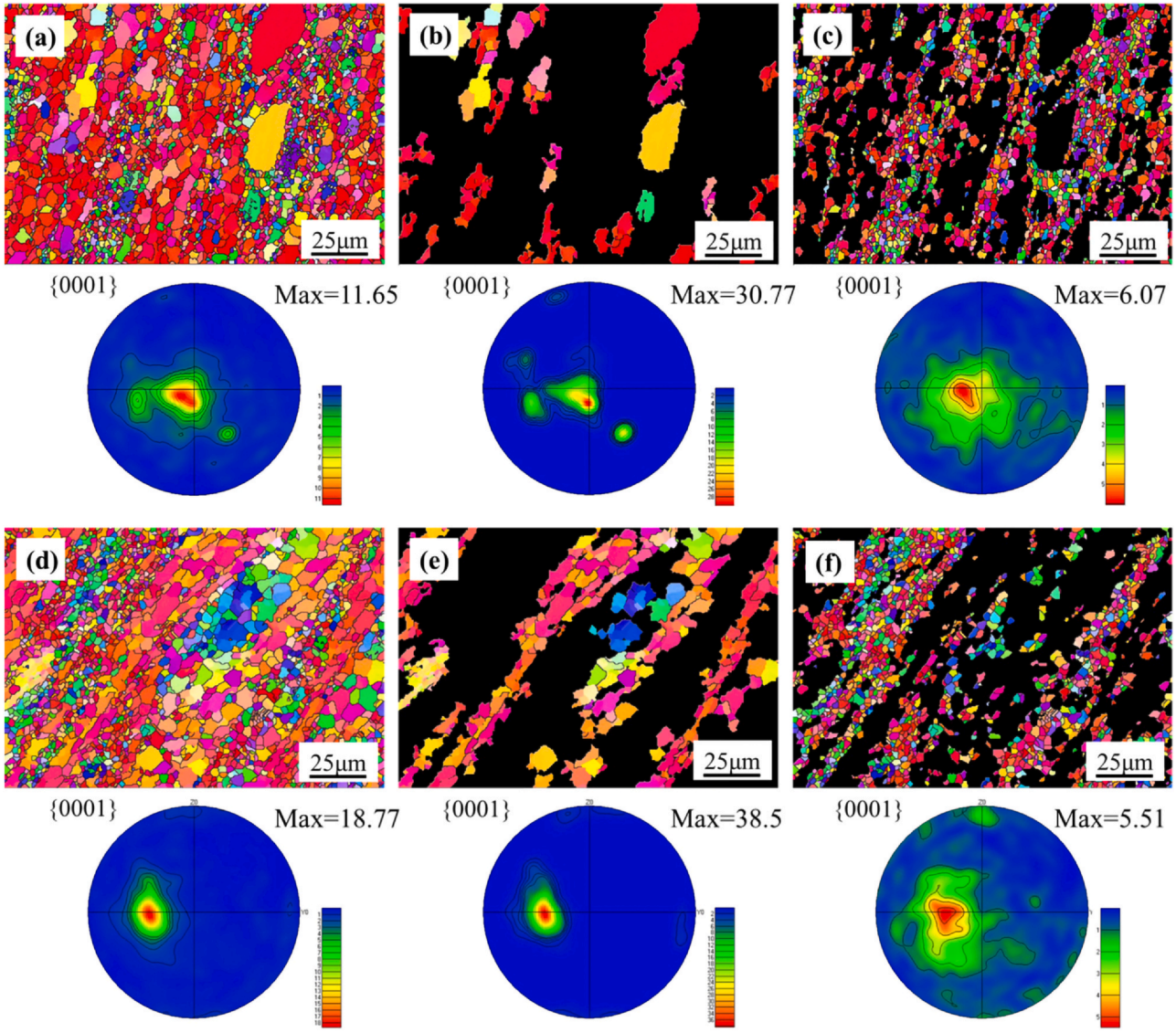


**Fig. 10.** Inverse pole figure maps and the corresponding pole figures with maximum intensity of ECAP alloys: (a) entire EBSD map, (b) large-grain domain, (c) fine-grain domain of 8p-ECAP Zn-Mg-Y alloy; (d) entire EBSD map, (e) large-grain domain, (f) fine-grain domain of 12p-ECAP Zn-Mg-Y alloy.

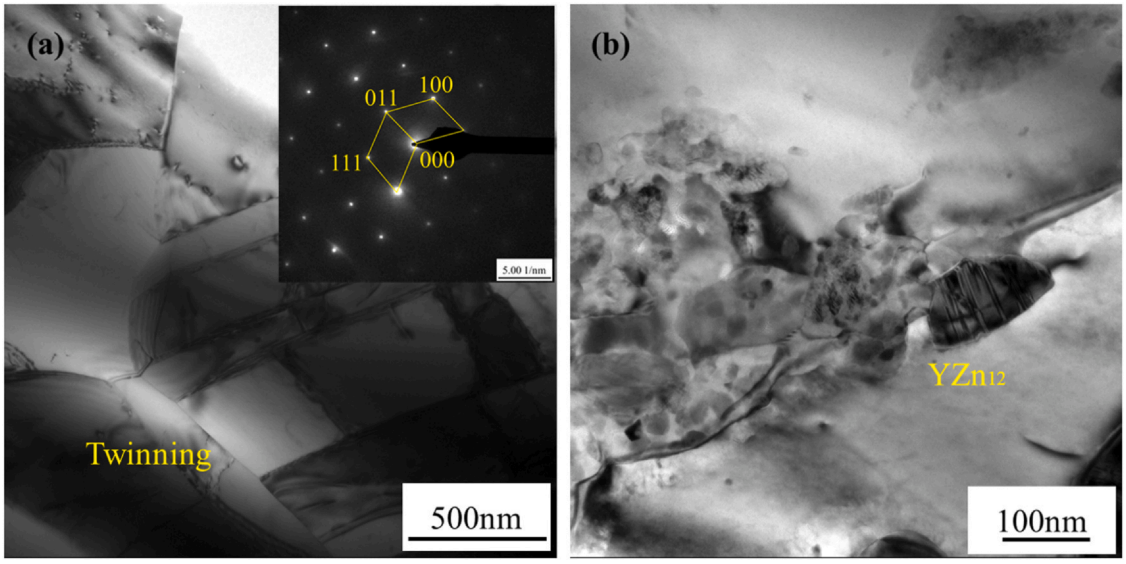


**Fig. 11.** TEM images of twinning structure in (a) Zn matrix, (b) $YZn_{12}$ phase.

observed only in the 12p-ECAP alloy. Therefore, the $YZn_{12}$ phase with twins in the 8p-ECAP alloy can hardly be observed, and it will make an important contribution to the ductility of 12p-ECAP Zn-Mg-Y alloy by reducing stress concentration at the interface related to the $YZn_{12}$ phase.

### *4.4. Work-hardening behavior in Zn-Mg-Y alloys processed by 12 passes of ECAP*

Softening behavior is a common phenomenon in Zn alloys owing to its low melting point, which could cause recrystallization during tension test at room temperature. Chen et al. [45] believe that the grain size of Zn alloys plays a critical role in work-hardening behavior by hinder boundaries slip. They found that Zn-Cu-Ag alloys with a grain size of 20 μm exhibit strain-hardening behavior under low strain below 15%, and the increase in grain size will result in a decrease of strength. In this study, the average grain sizes of 8p and 12p ECAP alloys are both about 3 μm, which is far below critical grain size. Therefore, the effect of refined second phases on work-hardening behavior in Zn alloys should be considered in this study. Based on the above analysis of microstructure during the ECAP process, it can be referred that the refined submicron-sized $YZn_{12}$ particles can inhibit recrystallization of Zn alloys via retarding the movement of (sub) grain boundaries. According to Zener pinning principle [46], recrystallization should not occur when $P_D^{Rex} < P_Z + P_C$, where $P_D^{Rex}$ is the driving force of recrystallization, $P_Z$ is Zener pressure, $P_C$ is the boundary curvature, and the $P_Z$ can be expressed as the following Eq. (3) [12]:

$$P_Z = \frac{3f_v\gamma_{AB}}{2r} \tag{3}$$

Where $f_v$ is the volume fraction of further refined submicron-sized $YZn_{12}$ phase, $\gamma_{AB}$ is the boundary tension and $r$ is the radius of submicron-sized $YZn_{12}$ particles. It is apparent that the value of $P_Z$ increases with increasing volume fraction and decreasing size of the submicron-sized $YZn_{12}$ particles. Therefore, the further refined submicron-sized $YZn_{12}$ phase with sizes near 100 nm in 12p alloy can effectively pin the grain boundaries and restrain the occurrence of recrystallization.

Work hardening is also related to the GND density, and the relationship can be expressed as the following Taylor Eq. (4) [47]:

$$\sigma_d = M\alpha Gb\rho^{\frac{1}{2}} \tag{4}$$

Where $\sigma_d$ is the contribution of dislocation density to flow stress, $M$ is Taylor factor, $\alpha$ is a constant, $G$ is shear modular (45 GPa), $b$ is Burgers vector (0.2664 nm) and $\rho$ is GND density. It can be seen from the Taylor equation that $\sigma_d$ increases with increasing GND density. The GND density can be calculated from the Kernel Average Misorientation (KAM) map which represents the local misorientation. Fig. 12 shows the KAW maps and the statistics distributions of local misorientation angle in 8p and 12p ECAP alloys. It can be observed that the peak in 8p alloy is slender than that in 12p alloy, which indicates that the statistic average value of 8p alloy is smaller than that of 12p alloy. The specific equation between average statistic value and GND density can be expresses as follows according to the strain gradient theory [48,49],

$$\rho^{GND} = \frac{2\Delta\theta_i}{ub} \tag{5}$$

where $\Delta\theta_i$ represents the local misorientation, $u$ is the unit length of the point (480 nm). It can be calculated that the $\Delta\theta_i$ of 8p alloy and 12p alloy are 0.49 and 0.62, respectively. The higher dislocation density in 12p alloy is attributed to the appearance of uniformly distributed $YZn_{12}$ particles and twins appeared within Zn matrix and refined submicron-sized $YZn_{12}$ particles. In our previous study [50], dislocations in Zn alloys could pile up at the grain boundaries and interface between Zn grain and $Mg_2Zn_{11}$ phase and generate radial dislocations via interaction between dislocations and precipitates. Therefore, the precipitates and twins in Zn-Mg-Y alloy after 12 passes of the ECAP process will hinder the movement of dislocations and increase the GND density of the grain interior. In a word, the further refined submicron-sized $YZn_{12}$ particles could improve the work-hardening ability of Zn alloys in two ways. On the one hand, they can pin the grain boundaries and inhibit the occurrence of recrystallization. On the other hand, they could increase the GND density markedly.

It is generally accepted that the high strength of Zn-Mg based wrought alloys is originated from the grain refienment and dispersion of $Mg_2Zn_{11}$ particles [25–28]. Our previous studies also confirmed that multi-pass ECAP is an effective method to refine matrix and eutectic structure, thus strengthening Zn-Mg alloys [23]. However, almost all Zn-Mg based alloys reported so far have displayed work softening after yielding, and work hardening is difficult to realize for Zn-Mg alloys. In this work, owing to the formation of furher refined submicron-sized $YZn_{12}$ particles with sizes of ~100 nm, which could induce twining within them and improve the

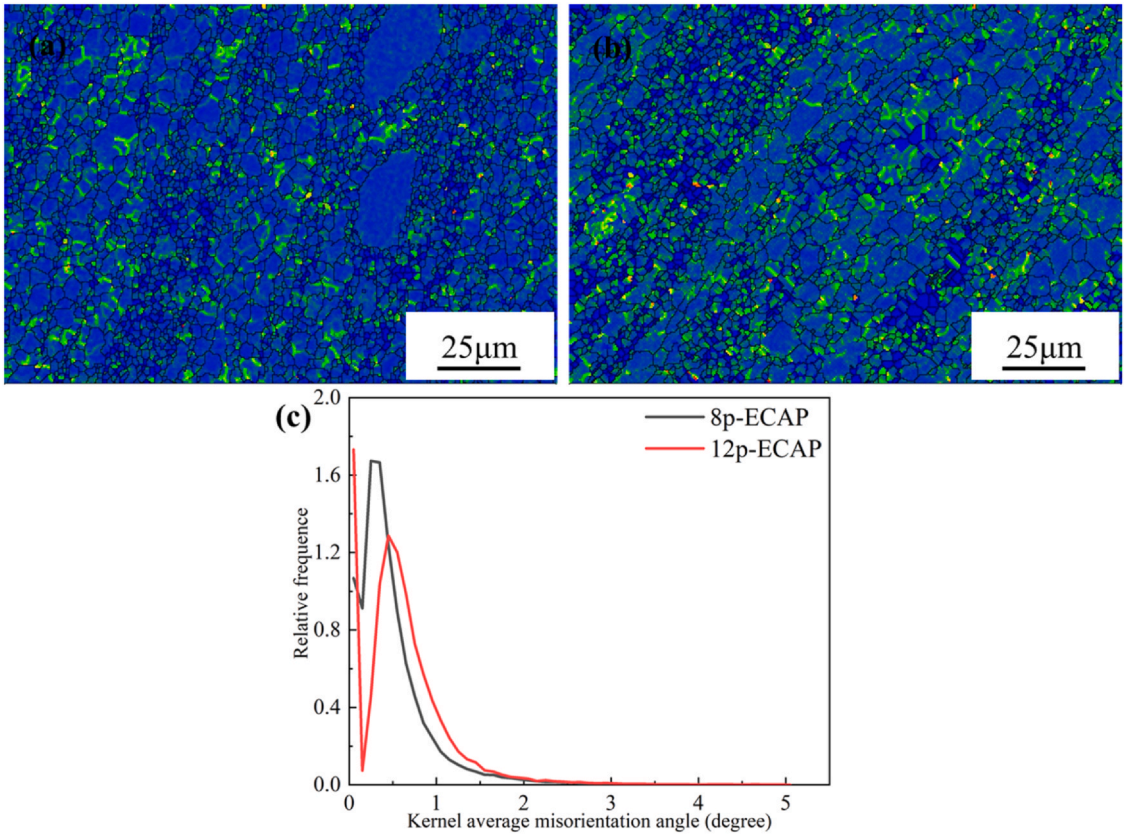


**Fig. 12.** KAM maps of: (a) 8p alloy, (b) 12p alloy, and (c) corresponding relative frequency.

GND density, the 12p Zn-Mg-Y alloy exhibits enhanced strength and ductility, together with strong work hardening ability. This study successfully proves that the formation of second phase particles with twinning ability could improve the work hardening ability of Zn alloys, which may provide a guidance for future alloy design.

## 5. Conclusions

In this paper, the effects of Y addition on microstructure evolution and mechanical properties, especially the ductility and work hardening ability of Zn-Mg-Y alloy during ECAP, were systematically investigated. The following conclusions can be drawn:

(1) The microstructure of as-cast Zn-Mg-Y alloy mainly consists of α-Zn matrix, network-shaped α-Zn + $Mg_2Zn_{11}$ + $MgZn_2$ eutectic structure, as well as micron-sized and submicron-sized $YZn_{12}$ particles.
(2) Multi-pass ECAP stimulates the occurrence of dynamic recrystallization and mechanical crushing of the eutectic structure gradually. $YZn_{12}$ particles exhibit no obvious change after 8p ECAP, while they are further refined from 8p to 12p-ECAP alloy, and submicron-sized $YZn_{12}$ particles near 100 nm in size were generated.
(3) Tensile test results show that the mechanical properties of Zn-Mg-Y alloys increase with increasing passes of ECAP. The 12p Zn-Mg-Y alloy possesses the best mechanical properties with ultimate tensile strength of 465 MPa and elongation of 11%. Moreover, the 12p ECAP alloy exhibit obvious work hardening ability.
(4) The further refined submicron-sized $YZn_{12}$ particles (~100 nm) are effective to inhibit boundaries slip and hinder the occurrence of recrystallization during tensile, and twinning occurred within Zn grains and $YZn_{12}$ particles could hinder dislocation movement to increase the GND density, all of which endow the 12p ECAP Zn-Mg-Y alloy strong work-hardening ability.

## CRediT authorship contribution statement

**He Huang:** Investigation, Writing - original draft, Visualization. **Huan Liu:** Supervision, Conceptualization, Writing - review & editing. **Kangxuan Ren:** Investigation. **Jiahui Shi:** Writing - review & editing. **Jia Ju:** Funding acquisition. **Haoran Wu:** Software, Methodology. **Jinghua Jiang:** Data curation. **Aibin Ma:** Data curation. **Feng Xue:** Visualization. **Jing Bai:** Supervision, Conceptualization. **Yufeng Zheng:** Supervision, Conceptualization.

## Declaration of Competing Interest

The authors declare that they have no known competing financial interests or personal relationships that could have appeared to influence the work reported in this paper.

## Acknowledgement

This work was supported by the National Natural Science Foundation of China (51901068), the Fundamental Research Funds for the Central Universities (B200203023, B200202131), and the Natural Science Foundation of Jiangsu Province of China (BK20181475).

## References

[1] P.K. Bowen, J. Drelich, J. Goldman, Zinc exhibits ideal physiological corrosion behavior for bioabsorbable stents, Adv. Mater. 25 (2013) 2577–2582.
[2] Y. Liu, Y.F. Zheng, X.H. Chen, J.A. Yang, H.B. Pan, D.F. Chen, L.N. Wang, J.L. Zhang, D.H. Zhu, S.L. Wu, K.W.K. Yeung, R.C. Zeng, Y. Han, S.K. Guan, Thermo-electro-mechanical vibrations of porous functionally graded piezoelectric nanoshells, Nanomaterials 9 (2019) 1805402.
[3] Y. Qin, P. Wen, D.D. Xia, H. Guo, M. Voshage, L. Jauer, Y.F. Zheng, J.H. Schleifenbaum, Y. Tian, Effect of grain structure on the mechanical properties and in vitro corrosion behavior of additively manufactured pure Zn, Addit. Manuf. 33 (2020) 101134.

[4] H.L. Jina, S. Zhao, R. Guillory, P.K. Bowen, Z.Y. Yin, A. Griebel, J. Schaffer, E.J. Earley, J. Goldman, J.W. Drelich, Novel high-strength, low-alloys Zn-Mg (< 0.1 wt% Mg) and their arterial Biodegradation, Mater. Sci. Eng. C 84 (2018) 67–79.

[5] L.Q. Wang, Y.P. Ren, S.N. Sun, H. Zhao, S. Li, G.W. Qin, Microstructure, mechanical properties and fracture behavior of as-extruded Zn-Mg binary alloys, Acta Metall. Sin. Eng. Lett. 30 (2017) 931–940.

[6] M.S. Dambatta, S. Izman, D. Kurniawan, S. Farahany, B. Yahaya, H. Hermawan, Influence of thermal treatment on microstructure, mechanical and degradation properties of Zn–3Mg alloy as potential biodegradable implant material, Mater. Des. 85 (2015) 431–437.

[7] C. Chen, J. Chen, W. Wu, Y. Shi, L. Jin, L. Petrini, L. Shen, G. Yuan, W. Ding, J. Ge, E.R. Edelman, F. Migliavacca, In vivo and in vitro evaluation of a biodegradable magnesium vascular stent designed by shape optimization strategy, Biomaterials 221 (2019) 119414.

[8] H.T. Yang, B. Jia, Z.C. Zhang, X.H. Qu, G.N. Li, W.J. Lin, D.H. Zhu, K.R. Dai, Y.F. Zheng, Alloying design of biodegradable zinc as promising bone implants for load-bearing applications, Nat. Commun. 11 (2020) 401.

[9] Z.Z. Shi, J. Yu, X.F. Liu, Twinning in MnZn13 intermetallic compound with base-centered monoclinic structure in Zn-0.75Mn alloy, Mater. Charact. 137 (2018) 9–13.

[10] H. Huang, H. Liu, L.S. Wang, K. Yan, Y.H. Li, J.H. Jiang, A.B. Ma, F. Xue, J. Bai, Revealing the effect of minor Ca and Sr additions on microstructure evolution and mechanical properties of Zn-0.6 Mg alloy during multi-pass equal channel angular pressing, J. Alloy. Compd. 844 (2020) 155923.

[11] J. Čapeka, J. Kubásek, J. Pinc, J. Maňák, O. Molnárová, J. Drahokoupil, M. Čavojský, ZnMg0.8Ca0.2 (wt%) biodegradable alloy – the influence of thermal treatment and extrusion on microstructural and mechanical characteristics, Mater. Charact. 162 (2020) 110230.

[12] K. Huang, K. Marthinsen, Q.L. Zhao, R.E. Logé, The double-edge effect of second-phase particles on the recrystallization behaviour and associated mechanical properties of metallic materials, Prog. Mater. Sci. 92 (2018) 284–359.

[13] H. Liu, J. Ju, X.W. Yang, J.L. Yan, D. Song, J.H. Jiang, A.B. Ma, A two-step dynamic recrystallization induced by LPSO phases and its impact on mechanical property of severe plastic deformation processed $Mg_{97}Y_2Zn_1$ alloy, J. Alloy Comp. 704 (2017) 509–517.

[14] J.N. Liu, D. Bian, Y.F. Zheng, X. Chu, Y.L. Lin, M. Wang, Z.F. Lin, M. Li, Y. Zhang, S.K. Guan, Comparative in vitro study on binary Mg-RE (Sc, Y, La, Ce, Pr, Nd, Sm, Eu, Gd, Tb, Dy, Ho, Er, Tm, Yb and Lu) alloy systems, Acta Biomater. 102 (2020) 508–528.

[15] Y.F. Zheng, X.N. Gu, F. Witte, Biodegradable metals, Mater. Sci. Eng. R Rep. 77 (2014) 1–34.

[16] K. Chen, Y. Lu, H.Y. Tang, Y.M. Gao, F. Zhao, X.N. Gu, Y.B. Fan, Effect of strain on degradation behaviors of WE43, Fe and Zn wires, Acta Biomater. 113 (2020) 627–645.

[17] Z.Z. Shi, W.S. Bai, X.F. Liu, H.J. Zhang, Y.X. Yin, L.N. Wang, Significant refinement of coarse (Fe, Mn)$Zn_{13}$ phase in biodegradable Zn–1Mn-0.1Fe alloy with minor addition of rare earth elements, Mater. Charact. 158 (2019) 109993.

[18] H. Huang, H. Liu, C. Wang, J.P. Wang, J. Bai, F. Xue, J.H. Jiang, A.B. Ma, Potential of multi-pass ECAP on improving the mechanical properties of a high-calcium-content Mg-Al-Ca-Mn alloy, J. Magnes. Alloy. 7 (2019) 617–627.

[19] J.P. Sun, Z.Q. Yang, J. Han, T. Yuan, D. Song, Y.N. Wu, Y.C. Yuan, X.R. Zhuo, H. Liu, A.B. Ma, Enhanced quasi-isotropic ductility in bi-textured AZ91 Mg alloy processed by up-scaled RD-ECAP processing, J. Alloy. Comp. 780 (2019) 443–451.

[20] H. Liu, C. Sun, C. Wang, Y.H. Li, J. Bai, F. Xue, A.B. Ma, J.H. Jiang, Improving toughness of a $Mg_2Ca$-containing Mg-Al-Ca-Mn alloy via refinement and uniform dispersion of $Mg_2Ca$ particles, J. Mater. Sci. Technol. 59 (2020) 61–71.

[21] H. Baker, ASM handbook, Alloy Phase Diagrams Vol. 3 ASM International, 1992.

[22] R.P. Elliott, First Suppl., 1965, 602–603.

[23] H. Liu, H. Huang, Y. Zhang, Y. Xu, C. Wang, J.P. Sun, J.H. Jiang, A.B. Ma, F. Xue, J. Bai, Evolution of Mg-Zn second phases during ECAP at different processing temperatures and its impact on mechanical properties of Zn-1.6Mg (wt%) alloys, J. Alloy. Compd. 811 (2019) 151987.

[24] H. Huang, H. Liu, L.S. Wang, Y.H. Li, S.O. Agbedor, J. Bai, F. Xue, J.H. Jiang, A high-strength and biodegradable Zn–Mg alloy with refned ternary eutectic structure processed by ECAP, Acta Metall. Sin. Engl. Lett. 33 (2020) 1191–1200.

[25] J. Kubásek, D. Vojtěch, E. Jablonská, I. Pospíšilová, J. Lipov, T. Ruml, Mechanical characteristics and in vitro degradation, cytotoxicity, genotoxicity and mutagenicity of novel biodegradable Zn-Mg alloys, Mater. Sci. Eng. C 58 (2016) 24–35.

[26] E. Mostaed, M. Sikora-Jasinska, A. Mostaed, S. Loffredo, A.G. Demir, B. Previtali, D. Mantovani, R. Beanland, M. Vedani, Novel Zn-based alloys for biodegradable stent applications: Design, development and in vitro degradation, J. Mech. Behav. Biomed. 60 (2016) 581–602.

[27] S.Y. Liu, D. Kent, N. Doan, M. Dargusch, G. Wang, Effects of deformation twinning on the mechanical properties of biodegradable Zn-Mg alloys, Bioact. Mater. 4 (2019) 8–16.

[28] J. Kubásek, D. Vojtěch, I. Pospíšilová, A. Michalcová, J. Maixner, Microstructure and mechanical properties of the micrograined hypoeutectic Zn-Mg alloy, Int. J. Min. Met. Mater. 23 (2016) 1167–1176.

[29] J.F. Hu, X.H. Wang, J.Z. Zhang, J. Luo, Z.J. Zhang, Z.J. Shen, Transform method in three-dimensional fluorescence spectra for direct reflection of internal molecular properties in rapid water contaminant analysis, Spectrochim. Acta Part A Mol. Biomol. Spectrosc. 250 (2021) 119376, https://doi.org/10.1016/j.jmat.2021.02.007

[30] H. Minkowski, Volumen und oberfläche, Math. Ann. 57 (1903) 447–495.

[31] J.W. Cahn, Significance of average mean curvature and its determination by quantitative metallography, Trans. Metall. Soc. AIME 239 (1967) 610.

[32] K. Hagihara, A. Kinoshita, Y. Sugino, M. Yamasaki, Y. Kawamura, H.Y. Yasuda, Y. Umakoshi, Effect of long-period stacking ordered phase on mechanical properties of Mg97Zn1Y2 extruded alloy, Acta Mater. 58 (2010) 6282–6293.

[33] H.B. Zhang, C.C. Zhang, B.K. Han, K.D. Gao, R.R. Fang, N.N. Deng, H.P. Zhou, Static recrystallization microstructure evolution in a cold-deformed Ni-based superalloy during electropulsing treatment, Crystals 10 (2020) 884.

[34] B. Guan, Y.C. Xin, X.X. Huang, P.D. Wu, Q. Liu, Quantitative prediction of texture effect on Hall–Petch slope for magnesium alloys, Acta Mater. 173 (2019) 142–152.

[35] H.H. Zhi, C. Zhang, S. Antonov, H.Y. Yu, T. Guo, Y.J. Su, Investigations of dislocation-type evolution and strain hardening during mechanical twinning in Fe-22Mn-0.6C twinning-induced plasticity steel, Acta Mater. 195 (2020) 371–382.

[36] R.X. Zheng, J.P. Du, S. Gao, H. Somekawa, S. Ogata, N. Tsuji, Transition of dominant deformation mode in bulk polycrystalline pure Mg by ultra-grain refinement down to sub-micrometer, Acta Mater. 198 (2020) 35–46.

[37] D.F. Lou, L.Q. Wang, Y.P. Ren, H.X. Li, G.W. Qin, Textural evolution and improved ductility in Zn-0.2Mg-0.8Mn (wt%) alloys at different extrusion temperatures, J. Alloy. Compd. 860 (2021) 158530.

[38] M.H. Yoo, Slip, twinning, and fracture in hexagonal close-packed metals, Metall. Trans. A 12 (1981) 409–418.

[39] X. Liao, J. Wang, J. Nie, Y. Jiang, P. Wu, Deformation twinning in hexagonal materials, MRS Bull. 41 (2016) 314–319.

[40] T.B. Britton, F.P.E. Dunne, A.J. Wilkinson, On the mechanistic basis of deformation at the micron-sized in hexagonal close packed metals, Proc. R. Soc. A (2015) 471.

[41] S.K. Oh, M.E. Kilic, J.B. Seol, J.S. Hong, A. Soon, Y.K. Lee, The mechanism of dynamic strain aging for type A serrations in tensile flow curves of Fe-18Mn-0.55C (wt%) twinning-induced plasticity steel, Acta Mater. 188 (2020) 366–375.

[42] J. Chan, C. Bruno, C. De, Temperature dependence of the flow stress of Fe–18Mn–0.6C–xAl twinning-induced plasticity steel, Acta Mater. 61 (2013) 6724–6735.

[43] S.N. Sun, Y.P. Ren, L.Q. Wang, B. Yang, H.X. Li, G.W. Qin, Abnormal effect of Mn addition on the mechanical properties of as-extruded Zn alloys, Mater. Sci. Eng. A 701 (2017) 129–133.

[44] H.T. Chen, Z.Z. Shi, X.F. Liu, Microstructure and mechanical properties of extruded and caliber rolled biodegradable Zn-0.8Mn-0.4Ag alloy with high ductility, Mater. Sci. Eng. A 770 (2020) 138543.

[45] C. Chen, R. Yue, J. Zhang, H. Huang, J.L. Niu, G.Y. Yuan, Biodegradable Zn-1.5Cu-1.5Ag alloy with anti-aging ability and strain hardening behavior for cardiovascular stents, Mater. Sci. Eng. C Mater. Biol. Appl. 116 (2020) 111172.

[46] C.S. Smith, Introduction to grains, phases, and interfaces: an interpretation of microstructure, Trans. Am. Inst. Min. Eng. 175 (1948) 15–51.

[47] X.H. Chen, F.S. Pan, J.J. Mao, J.F. Wang, D.F. Zhang, A.T. Tang, P. Jian, Effect of heat treatment on strain hardening of ZK60 Mg alloy, Mater. Des. 32 (2011) 1526–1530.

[48] H. Gao, Y. Huang, W.D. Nix, J.W. Hutchinson, Mechanism based strain gradient plasticity I. Theory, J. Mech. Phys. Solids 47 (1999) 1239–1263.

[49] L.P. Kubin, A. Mortensen, Geometrically necessary dislocations and strain-gradient plasticity: a few critical issues, Scr. Mater. 48 (2003) 119–125.

[50] H. Huang, H. Liu, L.S. Wang, K.X. Ren, K. Yan, Y.H. Li, J.H. Jiang, A.B. Ma, F. Xue, J. Bai, Multi-interactions of dislocations and refined microstructure in a high strength and toughness Zn-Mg-Mn alloy, J. Mater. Res. Technol. 9 (2020) 14116–14121.